Pattern Recognition 144 (2023) 109887

Contents lists available at ScienceDirect

Pattern Recognition

journal homepage: www.elsevier.com/locate/pr

A Gaussian kernel for Kendall's space of m-D shapes

Vicent Gimeno i Garcia [a], Ximo Gual-Arnau [b,*], M. Victoria Ibáñez [a], Amelia Simó [a]

[a] Department of Mathematics- IMAC. Universitat Jaume I. Castelló., Spain
[b] Department of Mathematics- INIT. Universitat Jaume I. Castelló., Spain

ARTICLE INFO

Keywords:
Riemannian manifold
Kendall shape space
Embedding
Reproducible Kernel Hilbert Space

ABSTRACT

In this paper, we develop an approach to exploit kernel methods with data lying on the m-D Kendall shape space. When data arise in a finite-dimensional curved Riemannian manifold, as in this case, the usual Euclidean computer vision and machine learning algorithms must be treated carefully. A good approach is to use positive definite kernels on manifolds to embed the manifold with its corresponding metric in a high-dimensional reproducing kernel Hilbert space, where it is possible to utilize algorithms developed for linear spaces. Different Gaussian kernels can be found in the literature on the 2-D Kendall shape space to perform this embedding. The main novelty of this work is to provide a Gaussian kernel for the m-D Kendall shape space. This new Kernel coincides in the case $m = 2$ with the Gaussian kernels most widely used in the Kendall planar shape space and allows to define an embedding of the m-D Kendall shape space into a reproducible kernel Hilbert space. As far as we know, the complexity of the m-D Kendall shape space has meant that this embedding has not been addressed in the literature until now. This methodology will be tested on a machine learning problem with a simulated and a real data set.

1. Introduction

The statistical analysis of the shapes of objects is of key importance in many scientific fields, such as Biology, Archaeology, Medicine, Geology, and Computer Vision and a great deal of research has been done in this field in recent decades. Three major approaches can be identified in Shape Analysis based on how the shape of the object is treated in mathematical terms: a multivariate vector of descriptive measures of shape, a sequence of points in the boundary of the object that are given by certain geometrical or anatomical properties (landmarks), or they can be described by using functions representing their contours. In this paper, we concentrate on the second approach, the case where the shape of an object is represented by a configuration matrix of landmarks. Seminal books on this subject are [1] for a practical point of view and [2] for a more theoretical mathematical study.

Formally, shape can be defined as the geometrical information about the object that is invariant under Euclidean similarity transformations, that is, location, orientation, and scale. The shape space is the resulting quotient space. When using the landmark-based approach, the corresponding shape space is a finite-dimensional curved Riemannian manifold, and statistical methodologies on manifolds have to be used.

Over recent decades, estimation and learning methods based on embedding data in a high-dimensional Reproducing Kernel Hilbert Space (RKHS) [3] have become rather popular, particularly in machine learning. See [4,5] for a review of the use of RKH spaces in the statistical and machine-learning contexts, and for active learning algorithms respectively. Traditionally, theory and algorithms of machine learning and statistics have been very well developed for the linear case. However, real-world data analysis problems often require nonlinear methods to detect the kind of dependencies that allow successful prediction or classification. By using a positive definite kernel, the RKHS theory allows us to embed our data in a (usually high dimensional) RKHS space (feature space) where the kernel corresponds to a dot product. In this space, our estimation methods are linear, and as long as we can formulate everything in terms of kernel evaluations, we never explicitly have to compute in the high-dimensional feature space.

When original data lie in a curved manifold, these algorithms provide an additional advantage: they can be applied in the RKHS in the same way that they are applied in the Euclidean case, without any adaptation, because, although the original space is curved, the feature space is not.

The great difficulty in using Hilbert space embeddings when the data are in curved Riemannian manifolds arises from the fact that the kernel function must be positive definite. Although many positive definite kernel functions defined for $\mathbb{R}^n$ are known, generalizing them to manifolds is not straightforward. In fact, it has been proved [6,7] that Gaussian kernels in curved spaces are never definite positive when geodesic distances are used. When considering the Kendall's space of m-D shapes, as far as we know, the space of planar shapes $m = 2$ is the only

* Corresponding author.
E-mail addresses: gimenov@uji.es (V.G. i Garcia), gual@uji.es (X. Gual-Arnau), mibanez@uji.es (M.V. Ibáñez), simo@uji.es (A. Simó).

https://doi.org/10.1016/j.patcog.2023.109887
Received 15 December 2022; Received in revised form 28 July 2023; Accepted 10 August 2023
Available online 15 August 2023

space that has been embedded in a reproducing kernel Hilbert space, which is because the proof is based on considering that the 2D Kendall shape space is the complex projective space, a relatively simple and familiar Riemannian manifold. However, for higher dimensions $m > 2$, the manifold structure of the corresponding shape spaces is rather more complex.

Our aim in this paper is to provide and prove a theorem that allows us to define a reproductive kernel in the Kendall shape space. When $m = 2$; that is, when planar curves are considered, the kernel we obtain generalizes and unifies two kernels widely used in the bibliography. In the case $m = 3$, that is surfaces in $\mathbb{R}^3$, this theorem allows us to propose a type of machine learning algorithm that we apply to two data sets: the support vector machine in the Kendall Shape Space.

Support vector machines (SVMs) are widely used machine learning algorithms for pattern recognition tasks, including classification and regression. They excel in scenarios involving high-dimensional data and the separation of distinct classes or groups. In the field of pattern recognition, the geometric properties of the Kendall shape manifold are sometimes exploited to apply SVM and other classification techniques. For example, in Human Action Recognition (HAR), one objective is to classify human actions using depth movies while representing the human body as dynamic skeletons in Kendall space [8]. Therefore, although this work makes contributions to the theory and methodology of pattern recognition, it also holds significant relevance in applications where data is represented in the shape space, as it enables the utilization of kernel methods in pattern design and recognition.

It is important to highlight that our proposed algorithm has potential for multimedia-related tasks such as image classification and video analysis. However, it assumes a preliminary stage of image and video preprocessing, where the Euclidean coordinates of the objects of interest are provided. While this may be perceived as a limitation, it also distinguishes our work from many existing algorithms that primarily focus on classifying shapes within images and videos. These algorithms often rely on alternative sources of information beyond point clouds or landmarks [9,10]. In contrast, our approach offers greater versatility, accommodating scenarios in biology, biomechanics, archaeology, and other domains where shapes can be obtained through direct scanning of objects [11] or manual annotation of their coordinates.

Some significant and recent bibliographic references on statistical learning in shape spaces are the following. Miolane et al. [12] introduce Geomstats, an open-source Python package for computations and statistics on nonlinear manifolds. Nava-Yazdani et al. [13] compute geodesic regression in Kendall's shape space. Xiao et al. [14] provides an overview of deep learning methods for shape analysis.

See [4] for a review of the use of reproducing kernel Hilbert spaces in the statistical and machine-learning context in Euclidean Spaces. Recently, several works have proposed to extend these approaches to Riemannian manifolds [6,7,15]. Concerning shape spaces, Jayasumana et al. [16] propose using positive definite kernels in the 2D Kendall shape space and de Carvalho and do Amaral [15] propose several methods based on the kernel trick also in this space.

Finally, regarding the state of the art on 3D shapes supervised classification based on landmarks, we must point out that references are scarce, since, as previously mentioned, most of the algorithms are designed only to classify shapes in images and videos, so many of them are based on other types of information than the point cloud or landmarks. Wang et al. [17], presents a dynamic graph convolutional neural network approach for learning on point clouds, which involves learning dynamic weights for the edges in the graph representation of the shape. The method is evaluated on several benchmark data sets and shown to achieve state-of-the-art performance on several tasks, including 3D shape classification and segmentation. Mirbauer et al. [18] proposes a deep learning approach for 3D shape classification using PointNet, a neural network architecture that directly processes point clouds. Wang et al. [17], presents a dynamic graph convolutional neural network approach for learning on point clouds, which involves learning dynamic weights for the edges in the graph representation of the shape. The method is evaluated on several benchmark data sets and shown to achieve state-of-the-art performance on several tasks, including 3D shape classification and segmentation. The performance of the PointNet algorithm will be compared with our approach in Section 6.4.

It should be noted that a strength of our method compared to these other existing methods is that these methods work with the reference points as belonging to a Euclidean space and therefore use linear approximations, whereas our method takes into account the curvature of the space.

Finally, we will also compare the performance of the approach proposed in this document with a classical supervised classification algorithm such as the k-Nearest Neighbor algorithm, which only requires the calculus of the distances between observations in the corresponding space.

The article is organized as follows: Sections 2 and 3 provide brief reviews of the theory of the Kendall m-D shape space and of the reproducible kernel Hilbert spaces, respectively. In Section 4 provides a new kernels for the m-D Kendall shape and defines the corresponding embedding, for the case $m = 2$ we relate two very widely used Gaussian kernels to embed the 2-D Kendall shape space in the RKHS. Section 6 contains the applied part of this paper. Finally, conclusions are discussed in Section 7.

2. Kendall m-D shape space

Each closed hypersurface that bounds an m-D domain can be identified by a set of landmarks, i.e., a set of points in the space $\mathbb{R}^m$ that identifies each object. In this section, we follow the notation introduced in [1].

Definition 1. A configuration matrix x is a $k \times m$ matrix with the Cartesian coordinates of the k landmarks of the boundary of an m-D domain.

The shape of an object is all the geometric information that remains invariant with translations, rotations, and changes of scale (similarity transformations). Thus:

Definition 2. The shape space Σ_m^k is the set of equivalence classes T_x of $k \times m$ configuration matrices $x \in \mathbb{R}^{mk}$ under the action of Euclidean similarity transformations.

Let x be a configuration matrix. We remove the location and scale effects, multiplying it by the Helmert submatrix, H [1], and dividing it by its Frobenius norm. So,

$$z_x = \frac{x_H}{\|x_H\|} \tag{1}$$

is called the pre-shape of the configuration matrix x.

In this way, all information about location and scale of x has been removed, but rotation information remains.

Definition 3. The pre-shape space S_m^k is the set of all possible pre-shapes.

S_m^k is a hypersphere of unit radius in $\mathbb{R}^{m(k-1)}$. The shape space, Σ_m^k, is the quotient space of S_m^k under rotations, i.e.

$$\Sigma_m^k = S_m^k / SO(m).$$

Let us denote by π the natural projection to the equivalence class,

$$\pi : S_m^k \to \Sigma_m^k.$$

A shape $[x]$ is an orbit associated with the action of the rotation group $SO(m)$ on the pre-shape.

When planar shapes are considered; that is, when the dimension $m = 2$, and the number of landmarks k that identify each closed plane curve

is greater than 2, it is well known [1] that the space of planar shapes Σ_2^k is a smooth manifold isometric to the complex projective space $\mathbb{CP}^{k-2}$ (without singular part). In this case, since $\mathbb{CP}^{k-2} = S_k^2/U(1)$, where S_k^2 is the pre-shape sphere and $U(1)$ the unitary group, complex coordinates can be used for the landmarks so that z denotes a complex $(k-1)$-vector in the pre-shape space S_k^2, and each planar shape is represented by the equivalence class $[z]$.

Under this representation of Σ_2^k, the full Procrustes distance between two shapes $[z_1]$ and $[z_2]$ is defined as follows:

$$d_{FP}([z_1],[z_2]) = \left(1 - |\langle z_1, z_2\rangle|^2\right)^{\frac{1}{2}}. \tag{2}$$

Note that we have considered starred coordinates according to [19], so the dimension of the vectors is $(k-1)$.

On the other hand, if $Gr(p,V)$ denotes the Grassmann manifold of all p-dimensional subspaces of the vector space V when $1 \le p \le \dim V$ (usually, $V = \mathbb{R}^n$ or $V = \mathbb{C}^n$), the Kendall's space of 2-D shapes Σ_2^k satisfies

$$\Sigma_2^k \cong \mathbb{CP}^{k-2} \cong Gr(1,\mathbb{C}^{k-1}) \subset Gr(2,\mathbb{R}^{2(k-1)}).$$

Then, a point on $\Sigma_2^k = Gr(1,\mathbb{C}^{k-1})$ is represented by an $(k-1)\times 1$ complex matrix $[z_1]$ where $\|z_1\| = 1$. That is, the point on $Gr(1,\mathbb{C}^{k-1})$ is the subspace (complex line) spanned by z_1 and the Projection distance between two subspaces (shapes) $[z_1]$, $[z_2]$ is given by

$$d_P([z_1],[z_2]) = \frac{1}{\sqrt{2}}\|z_1 z_1^* - z_2 z_2^*\|_F, \tag{3}$$

where * denotes the conjugate transpose and $\|A\|_F = \mathrm{trace}(A^*A)$.

3. Reproducible kernel Hilbert spaces

A Hilbert space can be considered as the natural generalization of the usual Euclidean spaces $\mathbb{R}^m$ and gives a framework to work with infinite-dimensional vectors as the limit of finite-dimensional ones. In particular, given an arbitrary set E, a RKHS is a Hilbert space of functions $f : E \to \mathbb{R}$ with some practical and interesting properties. The abstract theory of Reproducible Kernel Hilbert Spaces was developed by Aronszajn [20]. One of the most important theoretical properties of an RKHS is that if two functions, f and g, are close in the Hilbert space norm, then $f(x)$ and $g(x)$ are close for all $x \in E$.

Definition 4. Let H be a Hilbert space of real-valued functions defined on E and $\langle\cdot,\cdot\rangle_H$ the inner product on H. A function $K : E\times E \to \mathbb{R}$, is said to be a reproducing kernel (rk) associated with H if it satisfies:

1. for every $x \in E$, $K(\cdot,x) \in H$.
2. K satisfies the "reproducing property"; that is, $\forall f \in H$ and $x \in E$

$$f(x) = \langle K(\cdot,x), f\rangle_H$$

The next theorem is a sort of converse to this:

Definition 5. A symmetric function $K : E\times E \longrightarrow \mathbb{R}$ is positive definite if $\forall N \ge 1$, $\forall (a_1,\dots,a_N) \in \mathbb{R}$, $\forall (x_1,\dots,x_N) \in E$,

$$\sum_{i,j=1}^{N} a_i a_j K(x_i,x_j) \ge 0.$$

Theorem 6. *If K is a symmetric and positive definite function on $E\times E$, then there is a unique Hilbert space of real-valued functions, H, such that K is the reproducing kernel (rk) associated with H.*

Moreover, there is a function (Kolmogorov decomposition) $\varphi : E \to H$ such that

$$K(x,y) = \langle \varphi(x), \varphi(y)\rangle_H. \tag{4}$$

It is essential to bear in mind that the proof of this theorem is based on constructing the space H through the completion of

$$H_0 := \mathrm{span}\{\sum_{i=1}^{N} \alpha_i k(\cdot,x_i)\, \alpha_i \in \mathbb{R},\ x_i \in E\} \subset H.$$

The RKHS H associated with the kernel K is the closure of H_0.

In the particular case where the set E is the Kendall space of planar shapes Σ_2^k two positive definite Gaussian kernels have been introduced on this manifold.

The Procrustes Gaussian kernel $K_{FP} : \Sigma_2^k \times \Sigma_2^k \longrightarrow \mathbb{R}$ is defined as:

$$K_{FP}([z_1],[z_2]) = \exp\left(-\gamma d_{FP}^2([z_1],[z_2])\right), \tag{5}$$

which is a positive definite kernel for all $\gamma > 0$, [16].

The Projection Gaussian kernel $K_P : \Sigma_2^k \times \Sigma_2^k \longrightarrow \mathbb{R}$ is defined as:

$$K_P([z_1],[z_2]) = \exp\left(-\gamma d_P^2([z_1],[z_2])\right), \tag{6}$$

which is a positive definite kernel for all $\gamma > 0$, [6].

Proposition 7. *Both kernels, the Procrustes Gaussian kernel and the Projection Gaussian kernel coincide; that is, $K_{FP}([z_1],[z_2]) = K_P([z_1],[z_2])$.*

Proof. Let ρ denote the angle such that $\cos\rho = |\langle z_1,z_2\rangle| = |z_1^* z_2|$, where z^* denotes the conjugate transpose of z. Then,

$$d_{FP}^2([z_1],[z_2]) = 1 - \cos^2\rho, \tag{7}$$

and $0 \le \rho \le \frac{\pi}{2}$ (Eq. (4.13) of [21]).

On the other hand, if θ denotes the principal (Jordan) angle [22] of $[z_1]$ and $[z_2]$ as lines in $Gr(1,\mathbb{C}^{k-1})$, then

$$d_P([z_1],[z_2]) = \sin\theta. \tag{8}$$

From [23], we have that $\rho = \theta$; therefore

$$d_{FP}^2([z_1],[z_2]) = 1 - \cos^2\rho = 1 - \cos^2\theta = \sin^2\theta = d_P^2([z_1],[z_2]), \tag{9}$$

and

$$K_{FP}([z_1],[z_2]) = K_P([z_1],[z_2]). \qquad \square \tag{10}$$

Starting from the previous kernels, it is possible to work in Kendall's space of planar shapes Σ_2^k using the Reproducible Kernel Hilbert Space defined by these kernels. However, for m-dimensional Kendall spaces Σ_m^k, no positive definite kernels are known. In the next section, we present the main theoretical result of the paper. This consists of embedding the space Σ_m^k in a Euclidean space, and then mapping the data to a RKHS where support vector learning algorithms are applied. This is particularly interesting when considering shapes in $\mathbb{R}^3$ (surfaces). Additionally, we will prove that if we particularize our kernel for $m = 2$ (planar shapes), we obtain the Projection Gaussian kernel K_P.

4. Main result: A Gaussian kernel via an embedding method in Kendall's m-D space.

Let z be a $(k-1)\times m$ pre-shape, $z \in \mathbb{R}^{m(k-1)}$ and $v = z^t$ with the following collection of column vectors

$$v = [v_1\ v_2\ \dots\ v_{k-1}] \quad \text{with} \quad v_i \in \mathbb{R}^m \quad i \in \{1,\dots,k-1\} \tag{11}$$

In order to obtain a positive definite kernel, we will make use of the following embedding $\rho : \mathbb{R}^{m(k-1)} \to \mathbb{R}^N$ with $N = \frac{k(k-1)}{2} + \binom{k-1}{m}$ given by the map

$$v \mapsto \rho(v) := \left(\frac{1}{\sqrt{2}}\langle v_i,v_i\rangle, \langle v_i,v_j\rangle, \det\left(v_{k_1}, v_{k_2}, \dots, v_{k_m}\right)\right),$$

where $i < j$, $k_1 < k_2 < \cdots < k_m$ with $i,j,k_i \in \{1,2,\dots,k-1\}$, and $\langle v_i,v_j\rangle$ stands for the usual scalar product of v_i and v_j.

It is worth noting that in the notation of [24] $\rho(v) = (v^t v, (\Lambda^m(v))^t)$ being $\Lambda^m(v)$ the mth exterior power.

Main Theorem. *For any positive kernel $K : \mathbb{R}^N \times \mathbb{R}^N \to \mathbb{R}$ on $\mathbb{R}^N$, the map*

$$\widetilde{K} : \Sigma_n^k \times \Sigma_m^k \to \mathbb{R}, \quad ([x],[y]) \mapsto \widetilde{K}([x],[y]) := K(\rho(x),\rho(y))$$

is a positive definite kernel on Σ_m^k and it is independent on the particular choose of x and y such that $\pi(x) = [x]$ and $\pi(y) = [y]$. In particular,

$$K([x],[y]) = e^{-\gamma\|\rho(x)-\rho(y)\|^2}, \tag{12}$$

is a positive definite kernel on Σ_m^k for any $\gamma > 0$.

In this paper, we focus on the Gaussian kernel because it is the generalization of the kernel introduced in [16] for planar shapes and, as is well known, it provides the best results in practice. A great list of other positive definite kernels on Σ_m^k could be defined because, as indicated before, it is straightforward to find positive definite kernels in $\mathbb{R}^N$. Some examples include: $K([x],[y]) = \rho(x)^T\rho(y)$, $K([x],[y]) = \left(\rho(x)^T\rho(y) + r\right)^m$, $r \geq 0, n \geq 1$ and $K([x],[y]) = e^{-\gamma\|\rho(x)-i\rho(y)\|}$, $\gamma > 0$.

Before proving the Main Theorem, we will deduce from it the following consequence for the particular case of $m = 2$.

Corollary 8. *In the Kendall space of planar shapes Σ_2^k, our kernel*

$$\widetilde{K} : \Sigma_2^k \times \Sigma_2^k \to \mathbb{R}, \quad ([x],[y]) \mapsto \widetilde{K}([x],[y]) := e^{-\gamma\|\rho(x)-\rho(y)\|^2}$$

coincides with K_P.

Proof. As we have explained in Section 2, for $m = 2$, the pre-shape space is a $(2k-3)$-dimensional sphere and $\Sigma_2^k = S_k^2/SO(2)$. Moreover Σ_2^k, when equipped with the quotient metric, is a isometric smooth manifold to $\mathbb{CP}^{k-2}$ equipped with the Fubini–Study metric (up to a scale factor).

Let $v, w \in \mathbb{R}^{2(k-1)}$, then,

$$v = \begin{pmatrix} v_1^1 & \cdots & v_{k-1}^1 \\ v_2^1 & \cdots & v_{k-1}^2 \end{pmatrix}, \quad w = \begin{pmatrix} w_1^1 & \cdots & w_{k-1}^1 \\ w_2^1 & \cdots & w_{k-1}^2. \end{pmatrix}$$

where, $v_i = (v_i^1, v_i^2)$, $w_i = (w_i^1, w_i^2)$, $i = 1, \ldots, k-1$.

If we consider the elements z_1 and z_2 in the pre-shape space obtained by expressing v and w using the following complex notation:

$$z_1 = \begin{pmatrix} v_1^1 + \mathbf{i}v_2^1 \\ v_2^1 + \mathbf{i}v_2^2 \\ \cdots \\ v_{k-1}^1 + \mathbf{i}v_{k-1}^2 \end{pmatrix}, \quad z_2 = \begin{pmatrix} w_1^1 + \mathbf{i}w_2^1 \\ w_2^1 + \mathbf{i}w_2^2 \\ \cdots \\ w_{k-1}^1 + \mathbf{i}w_{k-1}^2 \end{pmatrix},$$

the Projection distance between their corresponding elements $[z_1], [z_2]$ in $\mathbb{CP}^{k-2}$ is computed as (3):

$$d_P([z_1],[z_2]) = \frac{1}{\sqrt{2}}\|z_1 z_1^* - z_2 z_2^*\|_F.$$

Now it is easy to check that

$$\|\rho(v) - \rho(w)\|^2 = \frac{1}{\sqrt{2}}\|z_1 z_1^* - z_2 z_2^*\|_F,$$

and, therefore,

$$\widetilde{K}([v],[w]) = K_P([z_1],[z_2]). \qquad \square$$

5. Proof of the Main Theorem

In this section we are proving the Main Theorem. More precisely, in this section we will state and prove Corollary 12 and Theorem 13. Corollary 12 implies that the map $i : \Sigma_n^k \to \mathbb{R}^N$ does not depend on the choice of representant of $[x]$. Namely, if $\pi(x) = \pi(y) = [x]$,

$$i([x]) = \rho(x) = \rho(y).$$

and moreover that $i : \Sigma_m^k \to \mathbb{R}^N$ is an injective map. Namely, $[x] = [y]$ if and only if $i([x]) = i([y])$. Finally, we will state and we will prove Theorem 13 which implies our Main Theorem.

5.1. Orbit space and invariants

Given $x \in S_m^k$, the orbit space $O_x \subset S_m^k$ of the group $SO(m)$ acting on S_m^k is given by

$$O_x := \{M\,x \ : \ M \in SO(m)\}.$$

Obviously, $y \in O_x$, if and only if, $\pi(x) = \pi(y)$.

An invariant of $SO(m)$ is a polynomial $p : \mathbb{R}^{m(k-1)} \to \mathbb{R}$ such that for any $A \in SO(m)$

$$p(v) = p(Av).$$

The set of invariant polynomials of $SO(m)$ will be denoted by $\mathbb{R}[\mathbb{R}^{m(k-1)}]^{SO(m)}$. An important tool in this setting is the following theorem.

Theorem 9 (*See [25], For Instance*)**.** *The invariants of $SO(m)$ separate the orbit space of $SO(m)$ acting on $\mathbb{R}^{m(k-1)}$.*

The meaning of the above theorem is that $y \in O_x$ (or equivalently, $\pi(x) = \pi(y)$) if and only if,

$$p(x) = p(y)$$

for any invariant $p \in \mathbb{R}[\mathbb{R}^{m(k-1)}]^{SO(m)}$. The space of invariant polynomials $\mathbb{R}[\mathbb{R}^{m(k-1)}]^{SO(m)}$ is finitely generated, and a generating set of $\mathbb{R}[\mathbb{R}^{m(k-1)}]^{SO(m)}$ made of homogeneous polynomials can be found in the following way:

Theorem 10. *Let z be a $(k-1)\times m$ pre-shape, $z \in \mathbb{R}^{m(k-1)}$ and $v = z^t$ with the following collection of column vectors*

$$v = [v_1\, v_2\, \ldots\, v_{k-1}] \quad \text{with} \quad v_i \in \mathbb{R}^m.$$

Given the action of $M \in SO(m)$ on $\mathbb{R}^{m(k-1)}$ defined by

$$v \mapsto Mv := [Mv_1\, Mv_2\, \ldots\, Mv_{k-1}]$$

a generating set of $\mathbb{R}[\mathbb{R}^{m(k-1)}]^{SO(m)}$ can be obtained as

$$\{p_{i,j}, q_{k_1,\ldots,k_m}\}$$

where the polynomials p, q are given by

$$p_{i,j}(v) = \langle v_i, v_j\rangle$$

$$q_{k_1,k_2,\ldots,k_m}(v) = \det\left(v_{k_1}, v_{k_2}, \ldots, v_{k_m}\right)$$

where $\langle v_i, v_j\rangle$ stands for the usual scalar product of v_i and v_j.

Remark 11. Since

$$p_{i,j}(v) = \langle v_i, v_j\rangle = \langle v_j, v_i\rangle = p_{j,i}(v)$$

for any $i, j = 1, \ldots, k-1$, we only need $\frac{k(k-1)}{2}$ of such invariants p. Moreover, due to the properties of the determinant, we only need $\binom{k-1}{m}$ of the q invariants. Hence we can give a generating setting of invariant polynomials of $SO(m)$ with $\frac{k(k-1)}{2} + \binom{k-1}{m}$ invariants.

Corollary 12. *Given $x, y \in S_m^k$ then $\pi(x) = \pi(y)$, if and only if,*

$$p_{i,j}(x) = p_{i,j}(y), \quad q_{k_1,\ldots,k_m}(x) = q_{k_1,\ldots,k_m}(y)$$

for any i, j, k_i from 1 to $k-1$.

5.2. Embedding the shape space in an Euclidean space

By using the invariant polynomials, we can provide an injective map

$$i : \Sigma_m^k \to \mathbb{R}^N$$

with $N = \frac{k(k-1)}{2} + \binom{k-1}{n}$, via the generating set of invariant polynomials, we will define the map

$$\rho : S_k^3 \to \mathbb{R}^N, \quad x \mapsto \rho(x) := \left(p_{i,j}(x), q_{k_1,\dots,k_m}(x)\right).$$

Since the invariant polynomials are fiber invariant, *i.e.*, if $\pi(x) = \pi(y)$ then $p(x) = p(y)$ for any invariant polynomial, the following map

$$i([x]) = \left(p_{i,j}(x), q_{k_1,\dots,k_m}(x)\right)$$

is well-defined, and any x can be used such that $\pi(y) = [x]$ ($y \in \pi^{-1}([x])$). Moreover, the following diagram

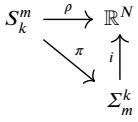

is a commutative diagram, and, furthermore, the map i defined above is an injective map. Effectively, if $i([x]) = i([y])$, then $\rho(x) = \rho(y)$ for any X, Y such that $\pi(x) = [x]$ and $\pi(y) = [y]$, but since $\rho(x) = \rho(y)$, then $p(x) = p(y)$ for any invariant polynomial, hence $[x] = \pi(x) = \pi(y) = [y]$.

5.3. Embedding the shape space in an RKHS Hilbert space

From the injective map $i : \Sigma_m^k \to \mathbb{R}^N$ described above, we have the following results.

Theorem 13. *Let $K : \mathbb{R}^N \times \mathbb{R}^N \to \mathbb{R}$ be a positive definite kernel. Then,*

$$\widetilde{K} : \Sigma_m^k \times \Sigma_m^k \to \mathbb{R}, \quad ([x],[y]) \mapsto \widetilde{K}([x],[y]) := K(i([x]), i([y]))$$

is a positive definite kernel on Σ_m^k.

Proof. We need to check that $\widetilde{K}$ is symmetric (*i.e.*, $\widetilde{K}([x],[y]) = \widetilde{K}([y],[x])$) but this is true because K is symmetric and hence

$$\widetilde{K}([x],[y]) = K(i([x]), i([y])) = K(i([y]), i([x])) = \widetilde{K}([y],[x]).$$

Moreover, we need to prove that

$$\sum_{i,j=1}^{l} c_i c_j \widetilde{K}([x]_i,[x]_j) = \sum_{i,j=1}^{l} c_i c_j K(i([x]_i), i([x]_j)) \geq 0$$

for all $l \in \mathbb{N}$, $\{[x]_1,\dots,[x]_l\} \subset \Sigma_m^k$ and $\{c_a,\dots,c_l\} \subset \mathbb{R}$. But this is true because K is positive definite. □

Once the main theorem has been proven, from Theorem 6, since a positive kernel has been defined in Σ_m^k, there is a map (Kolmogorov decomposition):

$$\varphi : \Sigma_m^k \longrightarrow H,$$

such that:

$$\widetilde{K}([x],[y]) = \langle \varphi([x]), \varphi([y]) \rangle_H . \tag{13}$$

In the machine learning literature, this map is called the feature map and allows us to embed our data in the RKHS H associated with the kernel K. The feature map is not unique, but the RKHS H of functions associated with K is. The most natural choice of φ is:

$$\Theta : \Sigma_m^k \longrightarrow H$$
$$[x] \mapsto \widetilde{K}(\cdot, [x]), \tag{14}$$

and it is called the canonical feature map, or the Aronszajn map. The proof of Theorem 6 of Section 3 states how the RKHS H associated with $\widetilde{K}$ is built. This result enables us to operate in a high-dimensional space without ever computing the coordinates of the data in that space, using methods that simply need to compute the inner products of all pairs of data. These methods include support vector machine, kernel k-means, and kernel PCA.

6. Applications

6.1. Experimental data sets

In order to illustrate the new framework proposed in this paper, two data sets will be used: a simulated data set and a real data set.

In order to obtain our simulated data set, we generate eight figures of a house with different shapes. Configurations $x_1,\dots,x_8$ are described by $k = 25$ landmarks. Fig. 1 shows the landmarks of these eight objects.

Then, random geometric objects are defined using a multivariate normal distribution with $3k$-dimensional mean vector $x_i, i = 1,\dots,8$ and a $3k \times 3k$ covariance matrix $\Sigma = 0.05 I_{k\times 3}$, i.e.:

$$\mathrm{vec}(x_{ji}|x_i) \sim N_{3k}(\mathrm{vec}(x_i), \Sigma).$$

This simulated study is the same as the one carried out in [26], where more details about the probability distribution of the shape of x_{ji} can be found.

Random samples of size 50, each with mean x_i $i = 1,\dots,8$, are obtained, resulting in a total random sample of size $n = 400$ (see Fig. 2).

We chose this dataset because it is easy to simulate, its probability distribution is well-established, and the resulting shapes have few landmarks, which allows tests to be carried out in a faster time and scale. Furthermore, using simulated data gives us greater control over the testing environment, enabling comprehensive and detailed testing in a controlled setting.

The second data set corresponds to the example in Section 1.4.3 of [1]. It consists of seven 3D anatomical landmarks located on the cranium of 9 males and 9 females, random sampled, of a specie of macaque (Macaca fascicularis). The seven landmarks are: 1, prosthion; 7, opisthion; 10, bregam; 12, nasion; 15, asterion; 16, midpoint of zyg/tems suture; and 17, interfrontomalare. An artist's impression is given in Fig. 3. We will use this data set to classify a new observation as male or female. The interest of the original study conducted by Paul O'Higgins [1] was to investigate if there are differences between sexes.

This is a very popular data set in the statistical shape analysis literature which has been used to illustrate and test many techniques such as geodesic PCA [27], clustering algorithms [28] and estimation of missing landmarks [29]. The data set is included in the R package shapes [21]. Fig. 4(a) and (b) shows the seven landmarks from a male and a female, respectively.

In both cases, we are faced with a problem of supervised classification on 3D shape spaces based on landmarks, and we propose to apply the support vector machine algorithm to solve both of them.

6.2. The support vector machine algorithm

The support vector machine (SVM) is one of the so-called kernel methods in the statistical learning literature [30]. As with all of them, it is based on the *kernel trick* that consists of embedding original data in the feature space H_K.

Given a training data set with $x_1,\dots,x_n$ configuration matrices and $y_i \in \{-1, 1\}$ associated labels, the fundamental idea of the binary SVM classification method is to find the hyperplane

$$w \cdot \varphi(x) + b = 0,$$

that separates the two classes such that the margin is maximized in the feature space H_K. The margin is defined as the distance between the hyperplane and the closest data points from each class. These data points are called support vectors, and the optimal hyperplane can be found by solving the dual optimization problem:

$$\texttt{maximize} \quad f(c_1,\dots,c_n) = \sum_{i=1}^{n} c_i - \frac{1}{2}\sum_{i=1}^{n}\sum_{j=1}^{n} y_i c_i K(x_i, x_j) y_j c_j \tag{15}$$

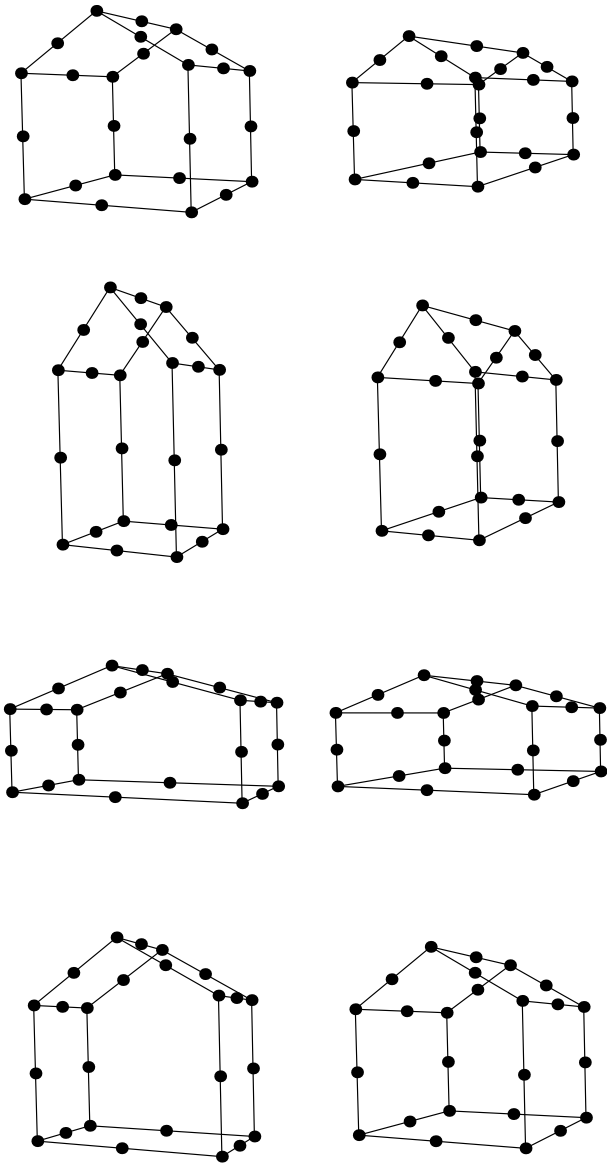

Fig. 1. Mean shapes.

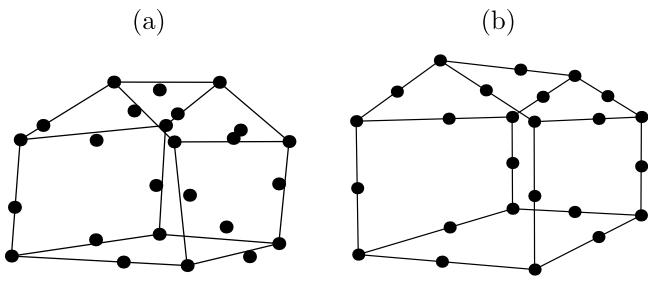

Fig. 2. (a) A simulated house and (b) the corresponding mean house.

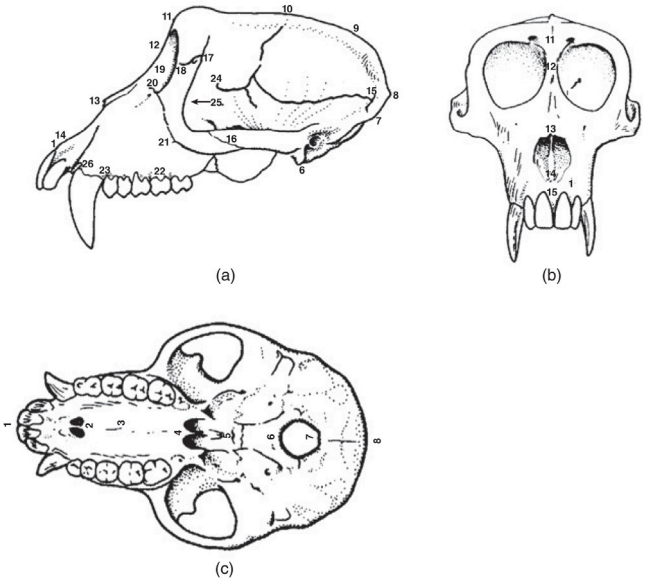

Fig. 3. A 3D macaque skull: (a) side view; (b) frontal view; and (c) bottom view. A total of 26 landmarks are displayed and a subset of 7 was taken for the analysis. *Source:* Taken from [1].

$$\texttt{subject to:}\quad \sum_{i=1}^{n} c_i y_i = 0,$$
$$0 \le c_i - \frac{1}{2nC} \ \forall i,$$

with

$$w = \sum_{i=1}^{n} c_i y_i \varphi(x_i)$$

and

$$b = \sum_{i=j}^{n} c_i y_i k(x_i, x_j), \tag{16}$$

for some i so that $\varphi(x_i)$ lies on the boundary of the margin. The parameter $C > 0$ determines the trade-off between increasing the margin size and ensuring that the $\varphi(x_i)$ lie on the correct side of the margin.

So, the SVM finds the optimal hyperplane in the feature space and uses it to make predictions on new data points, getting the position of these data points with respect to the hyperplane obtained.

SVM represents an extension of the maximum-margin hyperplane linear classifier algorithm developed by Vapnik [31]. It is one of the most robust prediction methods and has been widely applied to solve problems in many different scientific disciplines.

A multiclass classification problem is usually solved by breaking it down into multiple binary classification problems.

6.3. Algorithm

To classify a new shape using our proposed procedure, the methodology explained in Section 2 is used to obtain a representant of the shape of each configuration matrix of our data set. Once the representant is obtained, the Gaussian Kernel stated in Eq. (12) is applied to each pair of representants. Finally, the SVM algorithm is applied.

This procedure is given in detail in Algorithm 1.

Algorithm 1.

1 $x_1, \ldots, x_n$ training set of configuration matrices, $y_i \in \{-1, 1\}$ associated binary labels, X_0 configuration matrix to be classified

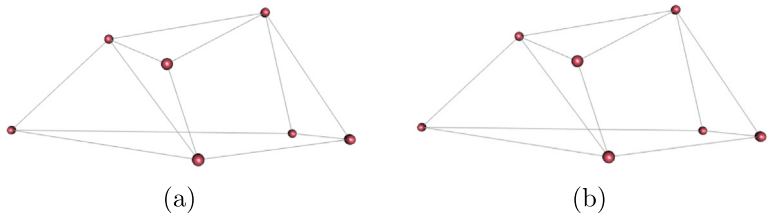

Fig. 4. The skull data with seven landmarks from a male macaque (a) and a female macaque (b).

Table 1
(a) Kernel support vector machine results for the simulated data set of houses with $C = 500$ using the full data set as training set. (b) results of the k-NN algorithm for different k-values.

Method		Training Accuracy	Training Precision	Training Recall	Training F1 score
SVM (a)		100%	100%	100%	100%
kNN (b)	$k = 3$	89.00%	89.00%	89.00%	88.98%
	$k = 6$	89.00%	89.06%	89.00%	88.89%
	$k = 13$	89.25%	89.37%	89.25%	89.06%
	$k = 17$	89.75%	89.82%	89.75%	88.66%

Table 2
Kernel support vector machine leave-one-out cross-validation results for the simulated data set of houses with $C = 500$.

Method	CV Accuracy	CV Precision	CV Recall	CV F1 score
$\gamma = 0.001$	89.00%	89.00%	89.00%	89.00%
$\gamma = 0.005$	88.00%	88.00%	88.00%	88.00%
$\gamma = 0.01$	87.75%	87.75%	87.75%	87.75%
$\gamma = 0.015$	87.25%	87.25%	87.25%	87.25%

2 For $i = 1$ to n

Compute z_i using Eq. (1).
Vectorize z_i, $v_i = vec(z_i)$
Calculate the vector $\rho(v_i)$ using Eq. (11)

3 For $i = 1, \dots, n$. For $j = i, \dots, n$

Calculate $K(v_i, v_j)$ using Eq. (12)

4 Apply SVM algorithm to obtain $c_1, \dots c_n$ i.e. to solve the optimization problem Eq. (15) and calculate b with Eq. (16)
5 Calculate $d_0 = \sum_{i=1}^{n} c_i y_i k(x_i, x_0) - b$
6 If $sign(d_0) < 0$ $y_0 = -1$, else $y_0 = 1$

For a multiclass classification problem steps 4, 5 and 6 are repeated for all possible binary classification problems.

6.4. Results

The previous algorithm (Algorithm 1), has been applied to our data sets. The preshapes z_i were directly obtained using the R package *shapes* [21] and the R package kernelab [32] was used to apply the SVM algorithm.

The most popular evaluation metrics have been used to evaluate our procedure: Accuracy, Precision, Recall and F1 score. Accuracy is defined as the ratio of the number of correct predictions to the total number of data. For a binary classifier system, Precision is the number of true positives divided by the number of total positive predictions. Recall is the number of true positives divided by the true positive and false negative. In other words, Accuracy represents the proportion of correct predictions overall, while precision measures the proportion of positive predictions that are truly positive, and recall measures the proportion of true positives that have been correctly identified by the model. The F1 score is the harmonic mean of Precision and Recall, i.e. maximizing the F1 score implies simultaneously maximizing Precision and Recall. These metric are extended to he case of a multiclass classification problem by decomposing it into a series of binary one-versus-remain problems and then averaging. All of them are used for the full data set (Training Accuracy, Training Precision, Training Recall and Training F1) and for a leave-one-out cross-validation study (CV Accuracy, CV Precision, CV Recall and CV F1).

The results for the simulated data set of houses (Fig. 1) can be seen in Tables 1 and 2 and the results for the macaque data set (Fig. 4) can be seen in Tables 4 and 5. Different values of parameter γ have been used.

In both cases, we have obtained excellent results, a perfect classification with training data has been obtained for all γ-values. Training Accuracy, Training Precision, Training Recall and Training F1 are all 100%.

In the case of the cross validation study, the results range with gamma.

For the macaque data set, the leave-one-out cross-validation accuracy increases with γ, and for $\gamma \geq 0.2$ the accuracy is 1.

However, for the simulated houses dataset, the leave-one-out cross-validation accuracy decreases as γ increases, and the variation of errors with gamma is much smaller. Although perfect classification is not achieved, the values of all metrics are quite high.

In both data sets, the values of Accuracy, Precision, and Recall are always very similar. This indicates that our procedure is able to accurately predict all classes most of the time

The results shown in Tables 1 and 4 allow us to compare the performance of our method and the k-NN algorithm. Since the k-NN algorithm calculates distances between all observations and does not specify a model, there is no process of parameter estimation involved. Therefore, proposing a leave-one-out cross-validation analysis in this scenario would be meaningless. We compute the Riemann distance between all pairs of points in both data sets [21] and then use these distance matrices to apply the k-NN algorithm for different values of k.

The k-NN algorithm does not achieve perfect classification with either of the two datasets (Tables 1 and 4). In both cases, the percentage of correct classifications with the k-NN algorithm are lower than that achieved with the SVM method. In the first case (Table 1), we obtain the best result for $k = 17$, while in the second database (Table 4) the best classification is obtained for $k = 6$.

Additionally, we apply the PointNet algorithm on our data sets. PointNet is a convolutional neural network specifically designed to handle point clouds, enabling various applications such as object classification, part segmentation, and scene semantic parsing.

To execute the algorithm, an implementation of "PointNet: Deep Learning on Point Sets for 3D Classification and Segmentation" [33] using PyTorch has been adapted to our databases. The original code is available on [34].

In our simulated database, we have 400 house simulations with landmarks, distributed across 8 distinct groups (50 simulations per group). For the training set, we randomly selected 35 houses from each group, leaving the remaining 120 houses (15×8) for the test set. After applying the PointNet algorithm, we obtained the normalized confusion matrix, displayed in Table 3. This matrix presents the predicted labels for the observations in the test set, alongside their true labels, and the

Table 3
Normalized confusion matrix for the simulated data set.

True/prediction	H1	H2	H3	H4	H5	H6	H7	H8
H1	0.20	0.27	0.07	0.20	0.20	0	0	0.07
H2	0.13	0.47	0.07	0.27	0.07	0	0	0
H3	0.20	0.40	0.07	0.07	0.07	0.20	0	0
H4	0.07	0.07	0.40	0.27	0.20	0	0	0
H5	0	0.07	0.80	0	0.13	0	0	0
H6	0	0	0.73	0	0.27	0	0	0
H7	0	0	0.60	0.33	0.07	0	0	0
H8	0	0	0	1	0	0	0	0

Table 4
(a) Kernel support vector machine results for the macaque data set with $C = 500$ using the full data set as training set. (b) Results of the k-NN algorithm for different k-values.

Method Method		Training Accuracy	Training Precision	Training Recall	Training F1 score
SVM (a)		100%	100%	100%	100%
kNN (b)	$k = 5$	0.67%	0.67%	0.66%	0.66%
	$k = 6$	77.78%	84.61%	77.77%	76.62%
	$k = 7$	72.22%	75.00%	72.22%	71.43%

Table 5
Kernel support vector machine leave-one-out cross-validation results for the macaque data set with $C = 500$ with a one-leave.

	CV Accuracy	CV Precision	CV Recall	CV F1 score
$\gamma = 0.05$	50.0000%	50.0000%	44.4444%	47.0588%
$\gamma = 0.1$	72.2222%	70.0000%	77.7778%	73.6842%
$\gamma = 0.15$	88.8888%	88.8888%	88.8888%	88.8888%
$\gamma = 0.2$	100%	100%	100%	100%

Table 6
Normalized confusion matrix for the macaque data set.

True/prediction	f	m
f	1	0
m	1	0

corresponding percentage of test observations. However, the percentage of correct classifications is relatively low in this case. In fact, the values of the metrics that we are evaluating in the different cases are now: Accuracy = 17.50%, Precision = 27.11%, Recall= 17.5% and F1 score = 21.15%.

The equivalent, in this case, of the one-leave-out CV method would be to train the neural network with all the data except one point and predict the class of that value using the trained network. This procedure would be iteratively repeated for all points in the dataset. We have applied this "one-leave-out" cross validation for the PointNET algorithm on the macaque data set. The normalized confusion matrix can be found in Table 6, and as can be seen, the algorithm cannot distinguish between males and females. Due to the limited number of observations and landmarks, the PointNET algorithm is ineffective in this case.

The poor classification results obtained by the PointNet algorithm in both data sets can be attributed to the fact that like other convolutional neural network algorithms, it requires a large number of training observations and a high number of landmarks per object to train the model and recognize the distinctive patterns of objects in each class.

In applications where obtaining a large number of observations or a high density of landmarks per observation is impossible, the PointNet algorithm tends to perform worse compared to our SVM-based algorithm.

In general, we find these results to be very satisfactory and promising.

7. Discussion

As is well known, the Kendall planar shape space is the complex projective space, a relatively simple and familiar Riemannian manifold. Until now, the projection metric has been widely used to define a positive definite Gaussian kernel (K_P) on this manifold to embed this space in a high-dimensional reproducing kernel Hilbert space, where it is possible to utilize algorithms developed for linear spaces. Alternatively, using the popular full Procrustes distance on the 2-D Kendall's shape manifold, a Gaussian kernel (K_{FP}) can also be defined for this embedding. Looking for a relationship between them, in Proposition 7 we have proven the equivalence of both kernels, i.e., that $K_{FP} = K_P$.

For $m > 2$, the m-D Kendall Shape space does not correspond to the complex projective space but to manifolds with rather more complex structures. As far as we know, this complexity has meant that the problem of embedding these spaces in an RKHS has remained as an unsolved problem until now. The main contribution of this paper has been to define a Gaussian kernel in the m-D Kendall Shape space that coincides with $K_{FP} = K_P$ for $m = 2$. This result enables us to operate in a high-dimensional space without ever computing the coordinates of the data in that space, using methods that simply need to compute the inner products of all pairs of data. These methods include support vector machine, kernel k-means, and kernel PCA. As an illustration, two problems of supervised classification have been proposed in Section 6. The support vector machine algorithm has been applied to solve both of them, achieving very satisfactory and promising results. Four popular metrics have been used for testing our procedure showing a high classification ability.

A possible weakness of our method is that if the shapes to be classified are contained in an image or video, a preprocessing step is required. However, this can also be considered a strength as it enables our method to be applicable in various other situations. In addition, our method takes into account the curvature of the space, and achieves good results despite a relatively small number of objects and landmarks.

The pattern recognition audience can benefit from this work in two ways. First, from a practical point of view, it can be applied to similar pattern classification tasks in different contexts. Second, from a methodological point of view, the proposed Gaussian kernel enables the exploration and development of new kernel-based methodologies in shape spaces for other types of pattern recognition than classification. In our opinion, this represents a very interesting and promising avenue for future research.

Declaration of competing interest

The authors declare that they have no known competing financial interests or personal relationships that could have appeared to influence the work reported in this paper.

Data availability

Data will be made available on request.

Acknowledgments

This work was supported by Project UJI-B2020-22 from Universitat Jaume I, Spain, under Grant DPI2017-87333-R from the Spanish Ministry of Science, Innovation and Universities, and under grant PID2020-115930GA-100 funded by Spanish Ministry of Science and Innovation.

References

[1] I.L. Dryden, K.V. Mardia, Statistical Shape Analysis: With Applications in R, vol. 995, John Wiley & Sons, 2016.
[2] D.G. Kendall, D. Barden, T.K. Carne, H. Le, Shape and Shape Theory, John Wiley & Sons, 2009.
[3] A. Berlinet, C. Thomas-Agnan, Reproducing Kernel Hilbert Spaces in Probability and Statistics, Springer Science & Business Media, 2011.
[4] S. Saitoh, Y. Sawano, Theory of Reproducing Kernels and Applications, Springer, 2016.

[5] C.-C. Chang, B.-H. Liao, Active learning based on minimization of the expected path-length of random walks on the learned manifold structure, Pattern Recognit. 71 (2017) 337–348.
[6] S. Jayasumana, R. Hartley, M. Salzmann, H. Li, M. Harandi, Kernel methods on riemannian manifolds with gaussian rbf kernels, IEEE Trans. Pattern Anal. Mach. Intell. 37 (2015) 2464–2477.
[7] A. Feragen, F. Lauze, S. Hauberg, Geodesic exponential kernels: When curvature and linearity conflict, in: Proc. IEEE Comput. Soc. Conf. Comput. Vis. Pattern Recognit, 2015, pp. 3032–3042.
[8] B. Amor, J. Su, A. Srivastava, Action recognition using rate-invariant analysis of skeletal shape trajectories, IEEE Trans. Pattern Anal. Mach. Intell. 38 (2016) 1–13.
[9] K. Al-Dulaimi, V. Chandran, K. Nguyen, J. Banks, I. Tomeo-Reyes, Benchmarking hep-2 specimen cells classification using linear discriminant analysis on higher order spectra features of cell shape, Pattern Recognit. Lett. 125 (2019) 534–541.
[10] P.L. Rosin, Classification of pathological shapes using convexity measures, Pattern Recognit. Lett. 30 (2009) 570–578.
[11] S. Barahona, X. Gual-Arnau, M.V. Ibáñez, A. Simó, Unsupervised classification of children's bodies using currents, Adv. Data Anal. Classif. 12 (2018) 365–397.
[12] N. Miolane, N. Guigui, A. Le Brigant, J. Mathe, B. Hou, Y. Thanwerdas, S. Heyder, O. Peltre, N. Koep, H. Zaatiti, et al., Geomstats: A python package for riemannian geometry in machine learning, J. Mach. Learn. Res. 21 (2020) 9203–9211.
[13] E. Nava-Yazdani, H.-C. Hege, T.J. Sullivan, C. von Tycowicz, Geodesic analysis in kendall's shape space with epidemiological applications, J. Math. Imaging Vision 62 (2020) 549–559.
[14] Y.-P. Xiao, Y.-K. Lai, F.-L. Zhang, C. Li, L. Gao, A survey on deep geometry learning: From a representation perspective, Comput. Vis. Media 6 (2020) 113–133.
[15] J.B. de Carvalho, G.J.A. do Amaral, Classification methods for planar shapes, Expert Syst. Appl. 151 (2020) 113320.
[16] S. Jayasumana, M. Salzmann, H. Li, M. Harandi, A framework for shape analysis via hilbert space embedding, in: Proc. IEEE Int. Conf. Comput. Vis, 2013, pp. 1249–1256.
[17] Y. Wang, Y. Sun, Z. Liu, S.E. Sarma, M.M. Bronstein, J.M. Solomon, Dynamic graph cnn for learning on point clouds, ACM Trans. Graph. 38 (2019) 1–12.
[18] M. Mirbauer, M. Krabec, J. Křivánek, E. Šikudová, Survey and evaluation of neural 3d shape classification approaches, IEEE Trans. Pattern Anal. Mach. Intell. 44 (2021) 8635–8656.
[19] D G Kendall, Shape manifolds, procrustean metrics, and complex projective spaces, Bull. Lond. Math. Soc. 16 (1984) 81–121.
[20] N. Aronszajn, Theory of reproducing kernels, Trans. Amer. Math. Soc. 68 (1950) 337–404.
[21] I.L. Dryden, shapes package, R foundation for statistical computing, 2021, URL: http://www.R-project.org, Contributed package, Version 1.2.6.
[22] A. Galántai, C. Hegedűs, Jordan's principal angles in complex vector spaces, Numer. Linear Algebra Appl. 13 (2006) 589–598.
[23] S. Berceanu, On the geometry of complex grassmann manifold, its noncompact dual and coherent states, Bull. Belg. Math. Soc. Simon Stevin 4 (1997) 205–243.
[24] T. Carne, The geometry of shape spaces, Proc. Lond. Math. Soc. 3 (1990) 407–432.
[25] E.B. Vinberg, Lie groups and algebraic groups, Springer Ser. Comput. Math. (1990).
[26] G. Quintana-Ortí, A. Simó, A kernel regression procedure in the 3d shape space with an application to online sales of children's wear, Statist. Sci. 34 (2019) 236–252.
[27] S. Huckemann, T. Hotz, A. Munk, Intrinsic shape analysis: Geodesic pca for riemannian manifolds modulo isometric lie group actions, Statist. Sinica (2010) 1–58.
[28] S. Asili, A. Mohammadpour, O.N. Arjmand, M. Golalizadeh, A comparative study of some clustering algorithms on shape data, J. Iran. Stat. Soc. (JIRSS) 20 (2021) 29–42.
[29] S.M. Shin, J.H. Kim, Y.-S. Choi, Estimation of missing landmarks in statistical shape analysis, Commun. Stat. Appl. Method. 30 (2023) 37–48.
[30] T. Hastie, R. Tibshirani, J.H. Friedman, J.H. Friedman, The Elements of Statistical Learning: Data Mining, Inference, and Prediction, vol. 2, Springer, 2009.
[31] V. Vapnik, Pattern recognition using generalized portrait method, Autom. Remote Control 24 (1963) 774–780.
[32] A. Karatzoglou, A. Smola, K. Hornik, M.A. Karatzoglou, Package Kernlab, CRAN R Project, 2019.
[33] C.R. Qi, H. Su, K. Mo, L.J. Guibas, Pointnet: Deep learning on point sets for 3d classification and segmentation, in: Proc. IEEE Comput. Soc. Conf. Comput. Vis. Pattern Recognit, 2017, pp. 652–660.
[34] N. Karaev, I. Nikulina, pointnet, 2020, URL: https://github.com/nikitakaraevv/pointnet.

Vicent Gimeno i Garcia received his Ph.D. from Jaume I University in 2012. He is an Assistant Professor and Researcher at the Mathematics Department and Institute of Mathematics and Applications of the Jaume I University. His research interests are in differential and Riemannian geometry, submanifolds, and the geometry of quantum states.

Ximo Gual-Arnau received his Ph.D. from the University of València in 1995. He is a full professor at the Mathematics Department since 2009 and a researcher at the Institute of New Imaging Technologies of the Jaume I University. His research interests encompass Riemannian geometry and integral geometry, stereology, and the application of geometric techniques for shape recognition and classification.

M. Victoria Ibáñez received her Ph.D. from Jaume I University in 2003. She is an Assistant Professor and Researcher at the Mathematics Department and Institute of Mathematics and Applications of the Jaume I University. Her research interests are in functional data analysis and its application in biomedicine, the analysis of 2D and 3D shapes, and statistical learning in artificial intelligence.

Amelia Simó received her Ph.D. from the University of Valencia in 1995. She is a Full Professor and Researcher at the Mathematics Department and Institute of Mathematics and Applications of the Jaume I University. Her research interests are in spatial statistics: random sets, point processes, geostatistics, and statistical analysis of shapes.